6

Two-pion exchange contributions: results

Numerical results of the model for the NN strong interaction described in the previous chapter will be presented here. Models describing the same physics based upon chiral perturbation theory, such as the works of Entem *et al.* [38, 39], Kaiser *et al.* [33] and Epelbaum [164, 165] will be used for comparison. The higher partial waves are only sensitive to medium and long range physics. The latter is given by the one-pion-exchange (OPE) contribution as is long known. The medium range nucleon-nucleon interaction is dominated by correlated two-pion-exchanges (TPE). It thus makes sense to consider first the results for the high partial waves. This also provides a qualitative test for the chiral dynamics in the two nucleon interaction. For the reproduction of the lower partial waves a proper description of the short range part of the NN interaction is required. In our model this is achieved by the inclusion of the ω meson, responsible for the short range repulsion, the ρ meson which ensures the proper splitting of the coupled waves and a few other heavy mesons. Within the one-boson-exchange model (OBE) the introduction of a scalar isoscalar boson was necessary in order to reproduce the attractive medium range NN central potential. An important part of the TPE contributions mimics the exact same physics which should lead to a sizable decrease of the σ-nucleon coupling constant (g_ϵ). In the following the direct and crossed boxes supplemented by the c_0 football and triangle diagrams will be called NLO diagrams or terms, while the c_1, c_3 and c_4 triangles plus the c_0c_4 football will be called NNLO diagrams or terms. However, our diagrams contain, besides the corresponding chiral perturbation theory terms, higher order recoil and relativistic corrections.

6.1 Phenomenological interpretation of the LECs

The values of the low energy coupling constants c_i (LECs) are not constrained by chiral symmetry and they have to be determined from a fit to the experimental πN or alternatively NN elastic data. In chiral perturbation theory based models for the pion-nucleon elastic scattering the c_1, c_3 and c_4 coupling constants enter already at order Q^2 and from an analysis based on such a model the following values have been obtained [166]: c_1=-0.64 GeV^{-1}, c_3=-3.90 GeV^{-1}, c_4=2.25 GeV^{-1}. At order Q^3 the analysis of the πN data is performed by considering observables that receive contributions only from tree

LEC	πN	NN	this work
c_1	-0.87 ... -1.53	-0.76	-0.81
c_3	-5.25 ... -6.20	-4.78 ... -5.08	-4.70
c_4	3.47 ... 3.61	3.92 ... 4.70	3.40

Table 6.1: The ranges of the LECs (in GeV^{-1}) extracted from πN and NN scattering data compared with the values used in this thesis.

graphs containing the c_i couplings and finite one-loop corrections but no contributions from the a priori unknown terms in $\mathcal{L}^{(3)}_{\pi N}$. The range of the LECs as determined from such Q^3 analysis [78, 150, 166, 167] is shown in Table (6.1).

The extraction of the LECs from elastic NN scattering data has been performed by the Nijmegen group and collaborators [122, 77]. In their approach, the chiral two-pion-exchange component of the long-range nucleon-nucleon interaction derived from the chiral Lagrangian together with the full electromagnetic interaction and the one-pion-exchange potential are used to solve the relativistic Schrödinger equation with boundary conditions. The model is fitted to the *pp* Nijmegen data base and in the process the c_i coupling constants are extracted. The value of the c_1 coupling is determined from its relation to the pion-nucleon sigma term $\sigma(0)$ for which a low value is chosen, $\sigma(0)$=35$\pm$5 MeV. Extracting it via a fitting procedure is unreliable, even though consistent with values obtained from the πN analysis: c_1=-4.4$\pm$3.4 GeV^{-1}. Results from this analysis are shown Table (6.1), along with the values we have adopted for the LECs in this thesis, namely the ones used in Ref. [164]. The statistical errors on the extracted values are of the order of 0.2...0.3 GeV^{-1} and are not included in the presented ranges.

The phenomenological interpretation of the values of the LECs has been presented by Bernard *et al.* in [78]. An effective Lagrangian with resonances chirally coupled to nucleons and pions has been employed. Local pion-nucleon operators can be generated by letting the resonance masses become very large while keeping the ratio of coupling constants to masses fixed. In this way the resonance degrees of freedom are decoupled from the effective theory keeping however the information about these particles in the numerical values of the LECs. By considering both baryonic (B) and mesonic (M) excitations, one can write

$$c_i = \sum_{B=\Delta,N^*,\ldots} c_i^{(N)} + \sum_{M=\sigma,\rho,\ldots} c_i^{(M)} \,. \tag{6.1}$$

The contribution of a isoscalar-scalar meson to the $c_{1,3}$ coupling constants can be deduced from a chiral model for $\pi\pi$ scattering, which contains two two-pion scalar-meson interactions: one chiral symmetric and one breaking the chiral symmetry spontaneously. Their coupling constants are denoted by $\bar{c}_d$ and $\bar{c}_m$ respectively. The contribution to the c_1 LEC has the form

$$c_1^\sigma = -\frac{g_\sigma\, \bar{c}_m}{m_\sigma^2} = -0.81\,\mathrm{GeV}^{-1}, \tag{6.2}$$

where g_σ is the coupling constant of the isoscalar-scalar meson to nucleons with the numerical value $g_\sigma^2/4\pi = 7.6$ (Fleischer-Tjon OBE model value); here $\bar{c}_m$=30 MeV. Assuming that the value of c_1 is entirely due to the scalar meson exchange (i.e. $c_1^\sigma = c_1$) the mass of that meson, m_σ, can be determined from the above relation: m_σ=602 MeV. This value is reasonably close to the value used in the Fleischer-Tjon OBE model: m_σ=570 MeV. The scalar meson contribution to c_3 is given by

$$c_3^\sigma = -\frac{2 g_\sigma \, \bar{c}_d}{m_\sigma^2} = 2\frac{\bar{c}_d}{\bar{c}_m} \, c_1^\sigma = -1.22 \, \mathrm{GeV}^{-1}, \tag{6.3}$$

using $\bar{c}_d$=23 MeV. The ρ vector-meson contribution to c_4 amounts to

$$c_4^\rho = \frac{\kappa}{4M} = 1.81 \, \mathrm{GeV}^{-1} \, , \tag{6.4}$$

where M is the nucleon mass and for the vector meson magnetic moment the value κ=6.8 has been used. The contributions of the Δ isobar to the LECs has been determined by using the isobar model and the SU(4) coupling constant relation. It is summarized by the expression

$$c_3^\Delta = -2 \, c_4^\Delta = -\frac{g_A^2 \, (m_\Delta - M)}{2[(m_\Delta - M)^2 - m_\pi^2]} = -3.83 \, \mathrm{GeV}^{-1}. \tag{6.5}$$

This value bares sizable uncertainties, since by using the Rarita-Schwinger formalism and varying the value of the off-shell parameter Z changes up to 20% are found. In the mentioned reference [78] contributions of the N^* (Roper) baryon resonance have also been evaluated but found to be numerically small. We summarize by listing the values of the LECs obtained by adding up the various contributions to each of them

$$\begin{aligned} c_1 &= c_1^\sigma = -0.81 \, \mathrm{GeV}^{-1} \, , \\ c_3 &= c_3^\sigma + c_3^\Delta = -5.05 \, \mathrm{GeV}^{-1} \, , \\ c_4 &= c_4^\rho + c_4^\Delta = 3.73 \, \mathrm{GeV}^{-1} \, . \end{aligned} \tag{6.6}$$

6.2 Potential in coordinate space

The relativistic matrix elements of the elastic scattering matrix T or of the quasipotential W can be reduced to a non-relativistic form (matrix elements in a two component spinor space) by making use of the expression of the Dirac spinors in terms of Pauli spinors. One can then pass from momentum space to coordinate space representation and obtain the expression of the NN interaction in the form of non-relativistic potentials. This is achieved by Fourier transforming momentum space amplitudes that are well behaved. Otherwise the finite range part of the interaction in the coordinate space can be obtained as a superposition of Yukawa potentials via a spectral function representation of the momentum space amplitudes [15, 33]. The general expression of the on-shell scattering amplitude in the center of mass frame of two nucleons has the general form

$$T(\vec{r}, s, t) = V_C(r) + \vec{\tau}_1 \cdot \vec{\tau}_2 W_C(r) + [V_S(r) + \vec{\tau}_1 \cdot \vec{\tau}_2 W_S(r)] \vec{\sigma}_1 \cdot \vec{\sigma}_2 \tag{6.7}$$

$$
\begin{aligned}
& +[V_T(r)+\vec{\tau}_1\cdot\vec{\tau}_2 W_T(r)]S_{12}+[V_{SO}(r)+\vec{\tau}_1\vec{\tau}_2 W_{SO}(r)]\vec{L}\cdot\vec{S} \\
& +[V_Q(r)+\vec{\tau}_1\cdot\vec{\tau}_2 W_Q(r)]Q_{12} \\
S_{12} &= 3(\vec{\sigma}_1\cdot\hat{r})(\vec{\sigma}_2\cdot\hat{r})-(\vec{\sigma}_1\cdot\vec{\sigma}_2) \qquad (6.8)\\
Q_{12} &= \frac{1}{2}[(\vec{\sigma}_1\cdot\vec{L})(\vec{\sigma}_2\cdot\vec{L})+(\vec{\sigma}_2\cdot\vec{L})(\vec{\sigma}_1\cdot\vec{L})] \qquad (6.9)
\end{aligned}
$$

with s and t denoting the spin and respectively isospin variables. Contributions to the two-pion exchange potential have been determined starting with the 50's [168, 169, 170, 171] and the 70's [13]. Terms originating in the direct or crossed box and sometimes the c_0 loop diagrams have been considered in these older studies while in [15] the starting point has been the elastic πN scattering amplitude. In the last decade the form of two-pion-exchange potential has been studied taking into account the constraints set by chiral symmetry on the allowed form of the interaction [30, 155, 172, 173]. The most comprehensive work in this direction has been done by Kaiser and collaborators [33, 36, 37] who have determined the nucleon-nucleon potential up to order $\mathrm{N^3LO}$ in chiral perturbation theory. Among other contributions, the one-loop two-pion exchange potential has been determined up to $1/M^2$ corrections for the NLO diagrams and $1/M$ corrections for the NNLO ones. Dimensional regularization has been used to extract the finite part of the divergent loop integrals. Polynomial terms in the momentum transfer have been neglected since they only give rise to zero range potentials. Their result for the two-pion-exchange potential will be used in this section for a comparison with the one-boson-exchange potential generated by the mesons that have been considered in the model of Fleischer and Tjon. This comparison will also serve as a quantitative illustration of the phenomenological interpretation of the LECs. The coordinate space form of the one-boson-exchange potential can be obtained, for example, from the work of Partovi and Lomon [13]. In that reference a local expression for the OBE potential is derived by making an expansion in terms of $\vec{q}^{\,2}/M^2$ of the relativistic amplitudes, where $\vec{q}$ is the relative three-momentum of the two nucleons in their center of mass system. The first two terms of this expansion are kept (static term plus $1/M^2$ corrections) and all terms proportional with the total energy (non-local terms) are ignored. The values of the coupling constants of mesons to nucleons are the ones listed in the line labeled OBE in Table (6.4). In the calculations of the phase shifts, in the later sections, the fully relativistic amplitudes are employed. The difference between them and those of Kaiser is given by higher order terms in the $1/M$ expansion as well as non-local terms, their magnitude being assumed to be reasonably small.

We start with the isoscalar central potential, which is given by [33]

$$
\begin{aligned}
V_C(r) &= \frac{g_A^2}{32\pi^2 f_\pi^4}\left\{\frac{3e^{-2x}}{r^6}\Big[2c_1x^2(1+x)^2+c_3(6+12x+10x^2+4x^3+x^4)\Big]\right. \\
&\quad -\frac{1}{\pi Mr}\Big[\frac{12m_\pi c_3}{r^5}[(30x+12x^3)K_0(2x)+(30+27x^2+4x^4)K_1(2x)] \\
&\quad \left.+6(2c_1+c_3)m_\pi^6 K_0(2x)\Big]\right\}, \qquad (6.10)
\end{aligned}
$$

with $x=m_\pi r$, m_π the pion mass while M is the nucleon mass and $K_n(x)$ is the modified Bessel function. In order to avoid lengthy expressions not all the terms are shown here,

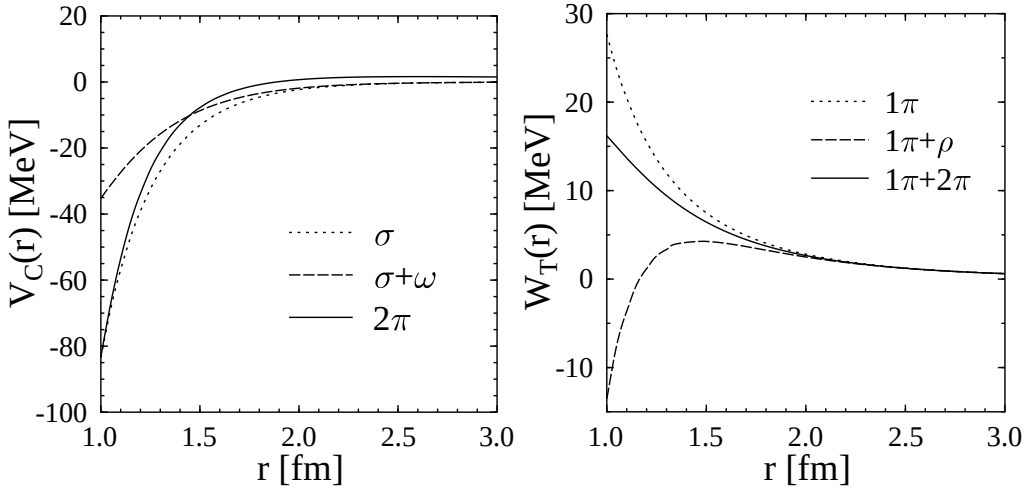

Figure 6.1: The isoscalar central potential $V_C(r)$ (left panel) and the isovector tensor potential $W_T(r)$ (right panel) generated by the one-loop two-pion exchange graph compared with the respective one-boson exchange potentials.

just the ones that are most important quantitatively. For example among the omitted terms are $1/M$ and $1/M^2$ contributions from the direct and crossed boxes and some $1/M$ corrections to the c_1 and c_3 triangles. The shown terms account for a strong short range attraction (first line) and strong short range repulsion (second line) and a long range repulsion (third line). This results in a net short range attraction which mimics very well the σ phenomenological short range attraction, while at long ranges the potential is repulsive, with a repulsion that amounts to 1 MeV at r=2.1 fm (see Fig. (6.1)). This last feature is opposite to the OBE model, which displays an attraction over the whole range of r. At N^{2}LO in chiral perturbation theory the dimensional regularized isoscalar central potential is far more attractive than the one presented here, at r=1 fm the attraction amounts to about 300 MeV. Epelbaum *et al.* [164] has shown that by using a sharp cut-off procedure to regularize divergent integrals, the resulting coordinate space central potential is in good agreement with the OBE one ($\sigma + \omega$) provided that the value of the cut-off is chosen in the range Λ=500...800 MeV.

The main contribution to the isovector-tensor potential comes from the c_4 triangle diagram and is attractive. Small corrections originating from the direct and crossed boxes and the c_0 diagrams are of the order of a few MeV. Compared with its phenomenological counterpart from the ρ meson the net attraction displayed by the TPE diagrams is about a factor 2 too small (Fig. (6.1)); $1/M$ corrections to the c_4 triangle are repulsive and quite large, of the order of 15 MeV at $r = 1$ fm. Comparing again with the finite cutoff result of [164] the attraction decreases even further when the value of the cutoff is chosen

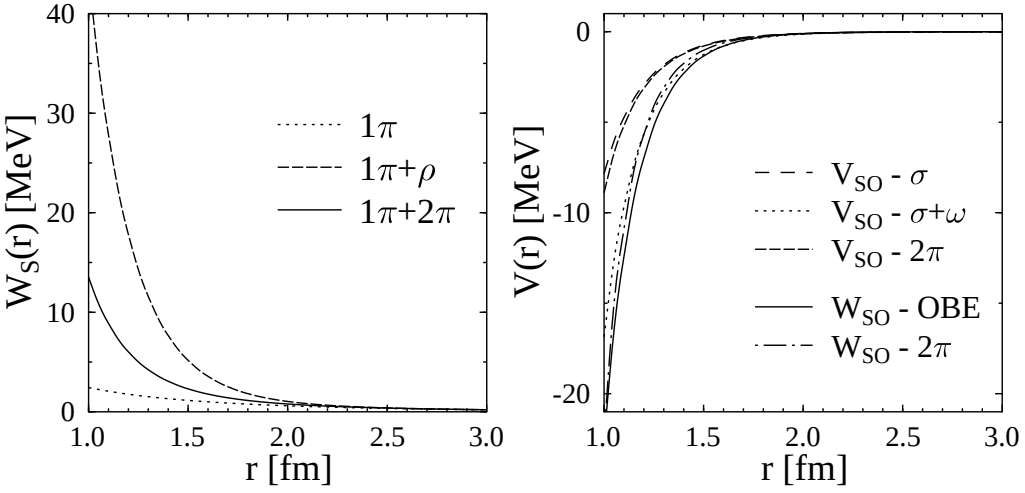

Figure 6.2: The isovector spin-spin potential W_C(r) (left panel) and the spin-orbit potentials V_{SO}(r) and W_{SO}(r).

as before. The dominant part of the two-pion isovector-tensor potential is given by

$$W_T(r) = -\frac{c_4 g_A^2}{48\pi^2 f_\pi^4 r^6}\left\{e^{-2x}(1+x)(3+3x+x^2)\right. \\ \left. -\frac{7m_\pi}{3\pi M}\Big[3x(8+x+2x^2)K_0(2x)+(24+21x^2+2x^4)K_1(2x)\Big]\right\}. \quad (6.11)$$

Turning to the isovector spin-spin potential, the c_4 triangle gives here the dominant contribution and as in the case of the isovector tensor potential the $1/M$ correction is important too. Smaller corrections, of the order of 1-2 MeV at r=1 fm, coming from the direct and crossed boxes and from the c_0 triangle and football graphs are included in Fig. (6.2). There is a large difference with respect to the OBE potential for which the ρ meson gives a strong repulsive spin-spin potential at short ranges. Nevertheless both potentials are repulsive and the difference between them reduces at bigger r given the shorter range of the ρ potential. Including a sharp cut-off [164] decreases the repulsion of the TPE potential at NLO in chiral perturbation theory. The c_4 triangle graphs contribution to the spin-spin potential has the following expression

$$W_S(r) = \frac{c_4 g_A^2}{48\pi^2 f_\pi^4 r^6}\left\{e^{-2x}(1+x)(3+3x+x^2)\right. \\ \left. -\frac{7m_\pi}{3\pi M}\Big[6x(5+2x^2)K_0(2x)+(30+27x^2+4x^4)K_1(2x)\Big]\right\}. \quad (6.12)$$

The isoscalar spin-orbit TPE potential receives contributions only from the direct and crossed box diagram. Besides these, in chiral perturbation theory at N^{3}LO, there is

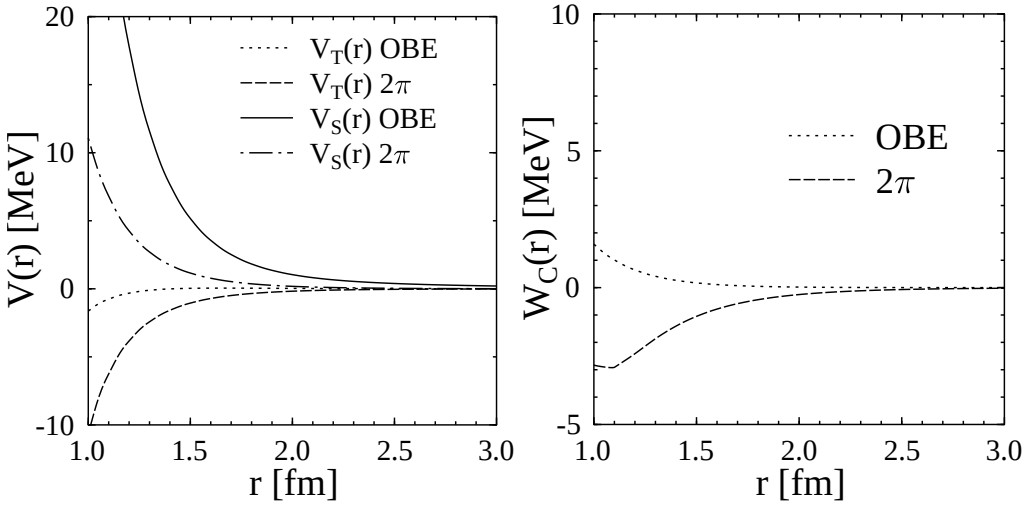

Figure 6.3: The isoscalar tensor (V_T(r)) and spin-spin (V_S(r)) potentials (left panel) and the isovector central potential W_C(r).

---

an $1/M$ correction to the c_2 diagram which gives an important repulsive contribution to the isoscalar spin-orbit potential [36]. It has not been taken into account here (together with a repulsive $1/M$ term contributing to the isoscalar scalar potential) since the c_2 interaction it not a part of our interaction Lagrangian. The considered terms give rise to a net attractive spin-orbit potential with a magnitude close to that of the σ meson (Fig. (6.2)). At short ranges ($r < 1.5$ fm) the ω leads to further attraction. The expression of the spin-orbit potential reads

$$\begin{aligned} V_{SO}(r) &= -\frac{g_A^4}{128\pi^2 f_\pi^4 r^6}\Big\{6e^{-2x}(1+x)(2+2x+x^2) \\ &\quad -\frac{m_\pi}{\pi M}\Big[x(165+52x^2)K_0(2x)+(165+132x^2+16x^4)K_1(2x)\Big]\Big\}. \end{aligned} \tag{6.13}$$

The main contributions to the isovector spin-orbit potential comes from $1/M$ corrections to the c_0c_4 football and the c_4 triangle. The latter dominates and is numerically close the ρ contribution (the contribution of the δ meson is negligible in this channel) to W_{SO} (Fig. (6.2)). The $1/M$ and $1/M^2$ corrections to the direct and crossed boxes and c_0 diagrams lead to a net attraction of about 2 MeV at r=1 fm [33]. The following expression is found for the dominating terms:

$$\begin{aligned} W_{SO}(r) &= \frac{3c_4 m_\pi}{4\pi^3 M f_\pi^4 r^6}\Big\{\Big[xK_0(2x)+(3+2x)K_1(2x)\Big] \\ &\quad +g_A^2\Big[x(15+4x^2)K_0(2x)+(15+12x^2)K_1(2x)\Big]\Big\}. \end{aligned} \tag{6.14}$$

These are the only TPE exchange potentials that in coordinate space show a clear connection with the corresponding one-boson potentials (σ, ω, ρ). For completeness we will present the expressions for the remaining two-pion-exchange potentials together with plots where the corresponding one-boson exchange potentials are also shown.

The one-boson-exchange isoscalar tensor potential comprises an attractive ω meson contribution and a repulsive η term which cancel each other to a large extent. The attractive net result is plotted in Fig. (6.3). At the two-pion exchange level there are only contributions from the direct and crossed boxes which are also attractive. Their expression is given by

$$\begin{aligned} V_T(r) &= \frac{g_A^4 m_\pi}{128\pi^3 f_\pi^4 r^4}\Big\{ -12xK_0(2x) - (15+4x^2)K_1(2x) \\ &+\frac{3\pi e^{-2x}}{8Mr}(\frac{12}{x}+24+20x+9x^2+2x^3) \\ &+\frac{1}{6M^2r^2}\Big[x(510+162x^2+8x^4)K_0(2x)+(510+417x^2+44x^4)K_1(2x)\Big]\Big\} \end{aligned} \tag{6.15}$$

The situation is somewhat similar in the case of the isoscalar spin-spin potential with both the ω and η mesons giving repulsive contributions. The TPE potential is again given by the contributions from the direct and crossed boxes which are repulsive this time. Their expression reads

$$\begin{aligned} V_S(r) &= \frac{g_A^4 m_\pi}{32\pi^3 f_\pi r^4}\Big\{3xK_0(2x)+(3+2x^2)K_1(2x) \\ &-\frac{2\pi e^{-2x}}{16Mr}\Big[\frac{6}{x}+12+11x+6x^2+2x^3\Big] \\ &+\frac{1}{6M^2r^2}\Big[x(90+36x^2+4x^4)K_0(2x)+(90+81x^2+14x^4)K_1(2x)\Big]\Big\} \end{aligned} \tag{6.16}$$

The isovector central potential is numerically small Fig. (6.3) due to a strong cancellation of attractive contributions originating in the direct and crossed boxes and a repulsive one due to the c_4 coupling. Both of these terms have an absolute magnitude of about 20 MeV. On the phenomenological side the repulsive ρ vector meson terms is dominating the small attractive contribution from the δ meson. The TPE isovector central potential has the form

$$\begin{aligned} W_C(r) &= \frac{g_A^2 m_\pi}{128\pi^3 f_\pi^4 r^4}\Big\{ -g_A^2(23+12x^2)K_1(2x) - g_A^2 x(23+4x^2)K_0(2x) \\ &+\frac{\pi e^{-2x}}{4Mr}\Big[2(3g_A^2-2)(\frac{1}{x}+12+10x+4x^2+x^3)+g_A^2x(2+4x+2x^2+3x^3)\Big] \\ &-\frac{g_A^2}{3M^2r^2}\Big[6x(135+43x^2+x^4)K_0(2x)+(810+663x^2+70x^4+4x^6)K_1(2x)\Big] \\ &+\frac{c_4}{Mr^2}\Big[12x(25+8x^2)K_0(2x)+4(50+41x^2+4x^4)K_1(2x)\Big]\Big\} \end{aligned} \tag{6.17}$$

To conclude this section we summarize the main similarities observed between the one-boson-exchange and the two-pion exchange. The σ meson potential is well reproduced in the isoscalar central channel by the c_1 and c_3 terms. The direct and crossed boxes contributions mimic to some extent the form of the ω potential in the isoscalar spin-orbit, tensor and spin-spin channels. Turning to the isovector potentials the c_4 terms give rise to a potential which has the right sign, but often the magnitude is a few times off (with the exception of the spin-orbit potential). It agrees with the presented results of the last section according to which only half of the value of c_4 has origin in the ρ meson physics . The quadratic spin-orbit terms have not been considered in this section. We have considered local one-boson-exchange potentials for which only the leading and next to leading local terms have been kept. To this order the one-boson-exchange potential has no quadratic spin-orbit terms. The TPE potential to N^{3}LO has only an isoscalar quadratic spin-orbit term coming from a $1/M^2$ correction to the direct+crossed boxes with a magnitude of about 1 MeV at r=1 fm [37]. The long range behavior of the TPE potential can be easily found by making use of the asymptotic behavior of the modified Bessel functions: $K_n(2x) \propto \sqrt{\frac{\pi}{2}} \frac{e^{-2x}}{\sqrt{2x}} \Big[1 + \mathcal{O}(1/2x)\Big]$.

6.3 Peripheral waves

Kaiser *et al.* [33] have shown that at NNLO in chiral perturbation theory, using dimensional regularization to extract the finite part of one-loop integrals, the peripheral waves for elastic scattering are reasonably reproduced up to 50 MeV for the D waves and up to 150 MeV for the higher partial waves. This poor convergence of the chiral expansion has been identified with the improper short range behavior of the NNLO diagrams, due especially to a strong central attraction caused by the c_3 triangle diagrams. This is mainly visible in the D and F waves, while the G waves and higher are dominated by one-pion-exchange. Epelbaum *et al.* [164] has shown that by using a sharp cut-off procedure with $\Lambda = 500 \ldots 800$ MeV the spurious short-range strong attraction of the NN potential at NNLO can be removed leaving a central potential which is of the same order of magnitude as the one obtained from the one-boson-exchange models. In the previous section, by putting together the NNLO [33] and N^{3}LO [36, 37] contributions to the one-loop two-pion-exchange potential is has been seen that at that order the strong attraction of the central potential has been reduced to values close to the σ meson contributions in the OBE model. This is however twice the size of the combined σ+ω attraction at r=1 fm. It is expected that by considering the full relativistic amplitudes the short-range central attraction to be milder.

We present the results for the peripheral waves for NN scattering for the model described in the previous chapter. The finite part of the loop integrals has been extracted via both dimensional and cut-off regularization. For the latter case a dipole form-factor has been chosen and the value of the cut-off Λ has been varied in the 632...782 MeV (the squares of these values expressed in nucleon masses "look simpler") range. With such values for the cut-off, contributions of ranges shorter than 0.5 fm are effectively left out. A disadvantage of a dipole form-factor with respect to a sharp one is that if a low value for the cut-off Λ is chosen the long range pieces of the potential are distorted to some extent.

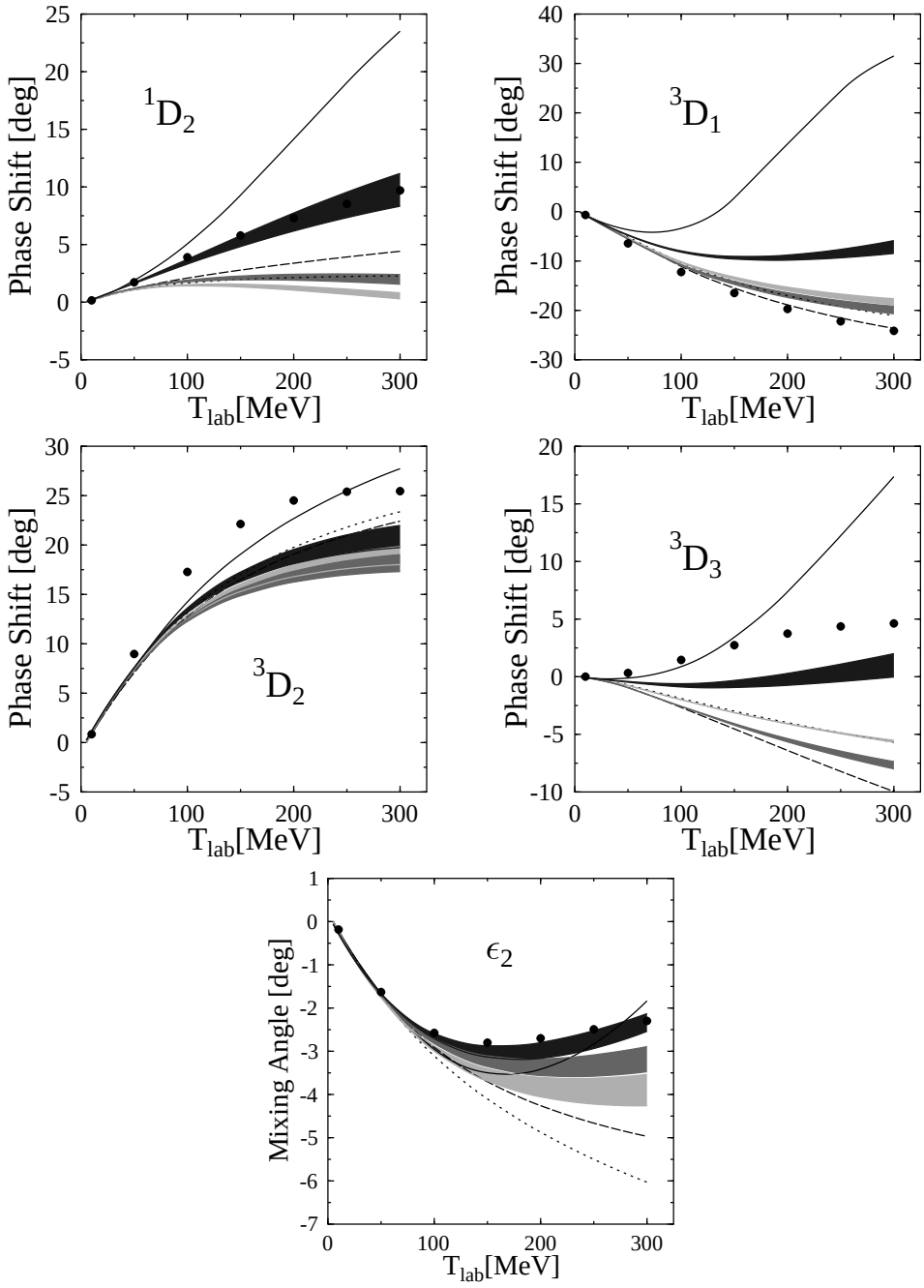

Figure 6.4: D-wave phase shifts and the mixing angle ϵ_2 as a function of the nucleon kinetic energy in the laboratory frame. The dotted, dashed and full curves are the dimensional regularization results for pure OPE (pointlike), NLO and NNLO respectively. The light-grey, grey and dark-grey bands correspond to a cutoff regularization calculation for the OPE, NLO and NNLO respectively. The PWA93 [121] experimental *np* phase shifts are shown for comparison.

Our choice here for a dipole cut-off is a necessity due to the particular way in which the diagrams are evaluated and due to a necessary compatibility with the one-boson-model to which the TPE potential will be added to determine the lower partial waves phase shifts. We remind here that the values used here for the LECs are the ones presented in Table (6.1). The value of the pion decay constant f_π=90.24 MeV has been determined from the Goldberger-Treiman relation using g_A=1.2573 and $g_\pi/4\pi^2$=13.6. To determine the phase shifts the matrix elements of the pseudo-potential W have been used, rather then the iterated T matrix. This is commonly accepted to be a good approximation for the higher partial waves as long as the value of the phase shift is small enough. At the Born level the scattering amplitude is real and extracting phase shifts (imposing a unitarity condition) introduces further approximations. We have extracted the phase shifts from the unitary representation of the partial wave amplitudes in Eq. (5.79)

$$\begin{aligned} T_J^J &= \frac{1}{2ik}\left[\exp(2i\delta_J)-1\right] \\ T_{J\pm1}^J &= \frac{1}{2ik}\left[\cos(2\epsilon_J)\exp(2i\delta_{J\pm1})-1\right] \\ T_{J,J\pm1}^J &= \frac{1}{2k}\sin(2\epsilon_J)\exp(i\delta_{J-1}+i\delta_{J+1}) \end{aligned} \tag{6.18}$$

by first computing $\tan\delta$ in order to avoid problems with inverse trigonometric functions. Our prescription is close to the one used by Kaiser [33], $T_J^J = \delta_J/k$, when the value of the extracted phase shift is small enough. The difference between the two amounts to at most 0.5° for the cases presented in this section.

We will start with the D waves, plotted in Fig. (6.4). The OPE result is a reasonable approximation only to the $^3D_1$ wave and to some extent to the $^3D_2$ wave. For the other waves the agreement is only qualitative: $^1D_2$ and ϵ_2 for which the sign is correctly reproduced but it is too weak and respectively too strong. In the case of the $^3D_3$ partial wave even the sign is different. These discrepancies are due to the sensitivity to TPE contributions and to iterations of the potential. The NLO contributions change the leading-order result with at most few degrees at T_{lab}=300 MeV for both the cut-off (CO) and dimensional regularization (DR) procedures. Main contributors at NLO are the direct ($^3D_2$,$^3D_1$ and $^3D_3$) and crossed ($^1D_2$ and ϵ_2) boxes. The c_0 diagrams are generally small, the only exception to that is in the $^3D_1$ where their repulsion increases the phase shifts with about 2° at 300 MeV. For the $^3D_2$ and $^3D_3$ partial waves these contributions are even in the wrong direction, most notably for the latter wave. A notable improvement is the values of ϵ_2 at higher energies while for the remaining waves the improvement is only marginal.

At NNLO a clear distinction has to be made between the CO and DR results. The former brings a notable improvement in all the partial waves with the exception of $^3D_1$ and perhaps $^3D_2$ which even though goes in the right direction the change is too small. The experimental values for $^2D_1$ and ϵ_2 fall now within the Λ =632...782 MeV bands and the results for the $^3D_3$ phase shifts have greatly improved. It is noteworthy that an improvement of the $^3D_2$ and $^3D_3$ would require a higher cut-off. The c_1 gives a isoscalar central attraction (see previous section) which has only a marginal impact on the D waves phase shifts. Important contributions to these waves at NNLO come from

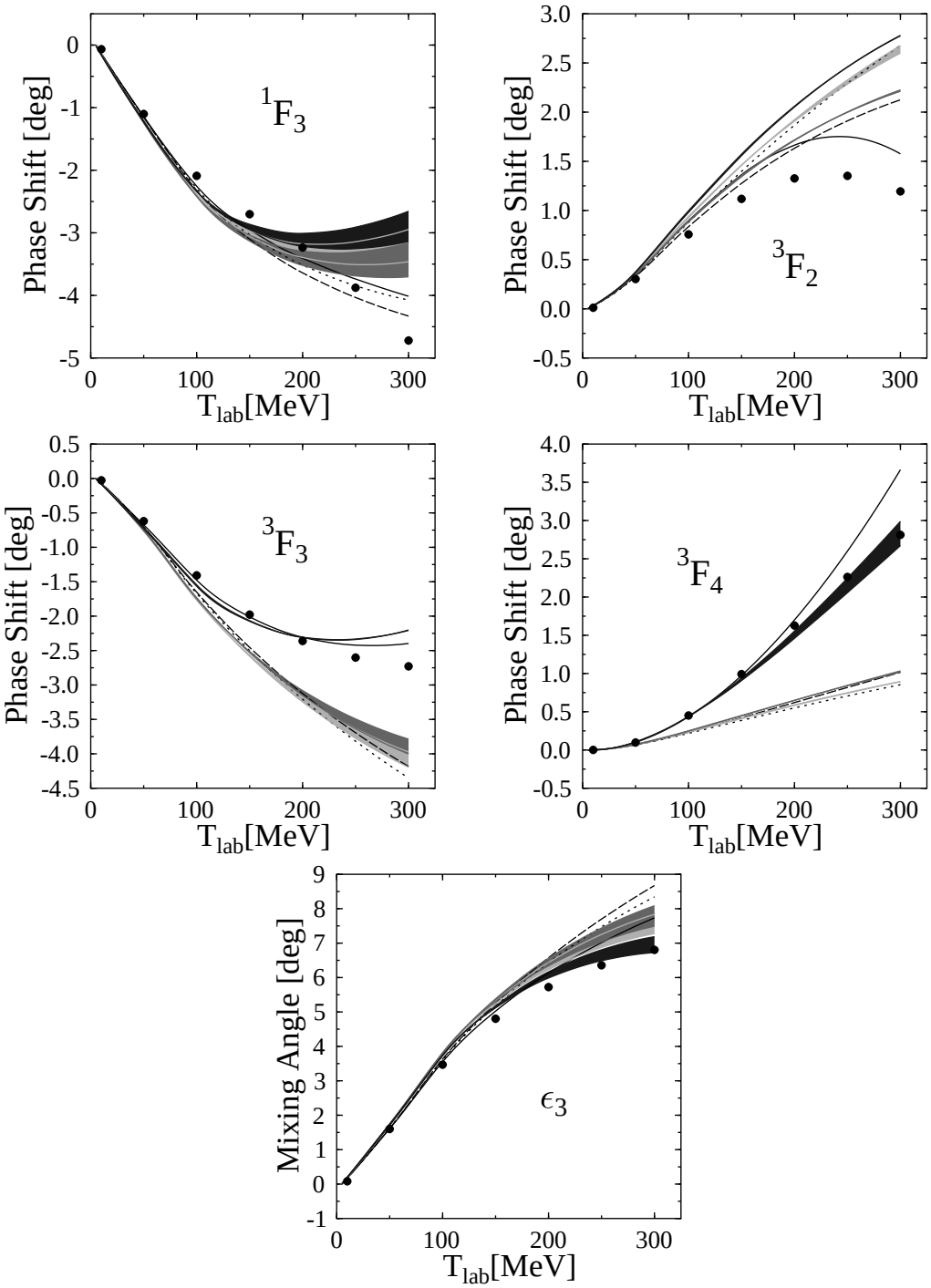

Figure 6.5: The same as in Fig. (6.4) but for the F waves and the ϵ_3 mixing angle.

	OPE	+DB	+CB	$+c_0$	$+c_1$	$+c_3$	$+c_4$	$+c_0c_4$
$^3D_1$	-16.03	-18.45	-18.37	-17.38	-17.23	-14.68	-9.63	-8.80
$^1D_2$	1.40	1.37	2.54	2.42	2.69	6.83	7.70	7.74
$^3D_2$	17.95	17.22	16.88	17.34	17.51	20.02	19.44	19.55
$^3F_2$	1.92	1.84	1.80	1.71	1.77	2.44	2.09	2.05
ϵ_2	-4.06	-3.96	-3.62	-3.56	-3.57	-3.98	-3.21	-3.16
$^1F_3$	-3.94	-3.43	-3.59	-3.52	-3.46	-2.67	-3.20	-3.22
$^3F_3$	-3.25	-3.28	-3.11	-3.15	-3.09	-2.34	-2.30	-2.31
$^3D_3$	-4.10	-5.64	-5.94	-5.65	-5.37	-0.62	0.38	0.29
$^3G_3$	-2.24	-2.41	-2.40	-2.35	-2.34	-2.19	-2.01	-1.99
ϵ_3	6.44	6.63	6.59	6.56	6.56	6.51	6.18	6.16
$^1G_4$	0.70	0.70	0.76	0.76	0.77	0.94	0.97	0.97
$^3G_4$	4.77	4.71	4.68	4.71	4.73	4.88	4.86	4.87
$^3F_4$	0.58	0.54	0.67	0.65	0.72	1.61	1.55	1.55
$^3H_4$	0.33	0.32	0.32	0.32	0.32	0.35	0.34	0.34
ϵ_4	-1.14	-1.14	-1.12	-1.12	-1.12	-1.12	-1.10	-1.10
$^3G_5$	-0.80	-0.89	-0.91	-0.90	-0.88	-0.70	-0.66	-0.67

Table 6.2: Contributions of the individual TPE diagrams at T_{lab}=200 MeV with the cut-off Λ^2=616 MeV^2. The result of each column is obtained by adding the mentioned contribution to the one in the neighboring left column. These manipulations were done at the level of scattering amplitudes and only then phase shifts were extracted. DB stands for the irreducible part of the direct box, c_0c_4 for the corresponding football diagram, etc.(see Section (5.6)).

---

the c_3 and c_4 diagrams which contribute most notably to central and respectively tensor potentials. It is the c_4 tensor attraction which is responsible for most of the discrepancy in the $^3D_1$ channel while for ϵ_2 the same attraction leads to agreement. The notable improvements in the $^1D_2$ and $^3D_3$ partial waves are due to the attraction generated by the c_3 term. A quantitative comparison of the contributions of each individual diagrams we have considered here is presented in Table (6.2). Phase shifts were extracted from the amplitude containing contributions from the diagram labeling the respective column plus all the diagrams labeling the columns to the left. By comparing the values in two neighboring columns the relative importance of each of the considered contributions at T_{lab}=200 MeV can be deduced. Turning to the DR results the first observation to be made is that they are far more attractive at higher energies than their CO counterpart. This statement holds for each D wave with the mention that in the case of $^3D_2$ and ϵ_2 this supplementary attraction leads to an agreement with the experimental phase shifts at high energies. Our DR results are qualitatively similar (*i.e.* show similar strong attraction at high energies) to earlier results of Kaiser [33] and Epelbaum [164] but quantitatively the differences are important. Both authors find the attraction to be so strong that the phase shifts reach 40° already at 200 MeV for most of the D waves. Our CO result is similar to the one of Epelbaum, the differences originating in the extra terms we include (relativistic and recoil corrections) and to the different cut-off scheme.

Turning to the F-waves (Fig. (6.5)) the first observation to be made is that the DR result does not show the strong attraction at high energies we have noticed in the case of the D-waves. The same feature has been observed by Kaiser [33] and Epelbaum [164] with the mention that their results show a high energy attraction for the $^3F_3$,$^3F_2$ and $^3F_4$ that overshoots our own by 2°-3°. The DR for the $^1F_3$ partial wave is close to the OPE result due to an almost perfect cancellation between the NLO and NNLO diagrams.

The OPE is a good approximation for all of these waves up to an energy of 100 MeV and for some of them even higher. NLO diagrams are unimportant up to 200 MeV and they only contribute at most half a degree at 300 MeV. An important attraction is generated in each of the F partial waves by the c_3 term which is compensated to some extent in the $^1F_3$ and $^3F_4$ channels by an isovector tensor repulsion originating in the c_4 diagrams. Out of the NNLO terms only these two show a noteworthy contribution. The mixing angle ϵ_3 suffers a decrease with respect to its NLO value of about 1° at 300 MeV due to the c_4 repulsion. Furthermore the cut-off dependence at high energies is far more reduced than for the D waves, in some case to almost no sensitivity as is the case of the $^3F_2$ and $^3F_3$ waves. With the exception of the latter all the F-waves ($+\epsilon_2$) are in good agreement with the experimental *np* phase shifts.

The G-wave phase shifts and the mixing angle ϵ_4 are plotted in Fig. (6.6). The difference between the DR and CO calculations has reduced even further. As expected the OPE is the major contributor, while the effect of the NLO diagrams is negligible, about 0.2° at 300 MeV. NNLO diagrams that have a visible impact on these waves are, as expected, the ones proportional with the c_3 and c_4 couplings constants. The value of the ϵ_4 mixing angle is determined reliably by the one-pion-exchange term. When comparing with the experimental values differences are found in the $^3G_3$ and $^3G_5$ channels. The differences, as relative values, are important and are due to the nonperturbative character of these waves. We will come back to this issue in a later section.

We have checked the results for even higher partial waves, namely H and I. At such a high value for the angular momentum contributions from short- or intermediate-range parts of the potential are expected to be marginal. This is what has been actually been observed: all of the partial waves and mixing-angles are determined with a high degree of accuracy by the long range part of the OPE potential. There is only one exception, the $^3H_6$ partial wave which receives an attractive contribution from the c_3 triangle diagram that increases the value of the corresponding phase shift by 60%. The resulting values of the phase shift are in excellent agreement with the experimental ones.

In the presented plots we have compared calculations obtained via dimensional- and cut-off regularization. To study the effect of a low cut-off on the short range part of the potential, strictly speaking, one should compare such a calculation with the one obtained by letting Λ grow to infinity, or at least to a large value. We have performed such a calculation too and present the cut-off sensitivity of the peripheral waves in Table (6.3). To demonstrate the sensitivity, results for phase shifts at T_{lab}=200 MeV for three values for the cut-off, Λ^2=1.67, 1.01 and 0.62 GeV^2, are shown. The last value corresponds to one of the limits of the low cut-off variation bands in the previous plots, while the first is high enough such that it corresponds to an almost pointlike ($\Lambda \to \infty$) pion-nucleon interaction. Two feature are readily observable: a higher sensitivity towards lower values of the cut-off (according to expectations) and that the main part of the cut-off sensitivity

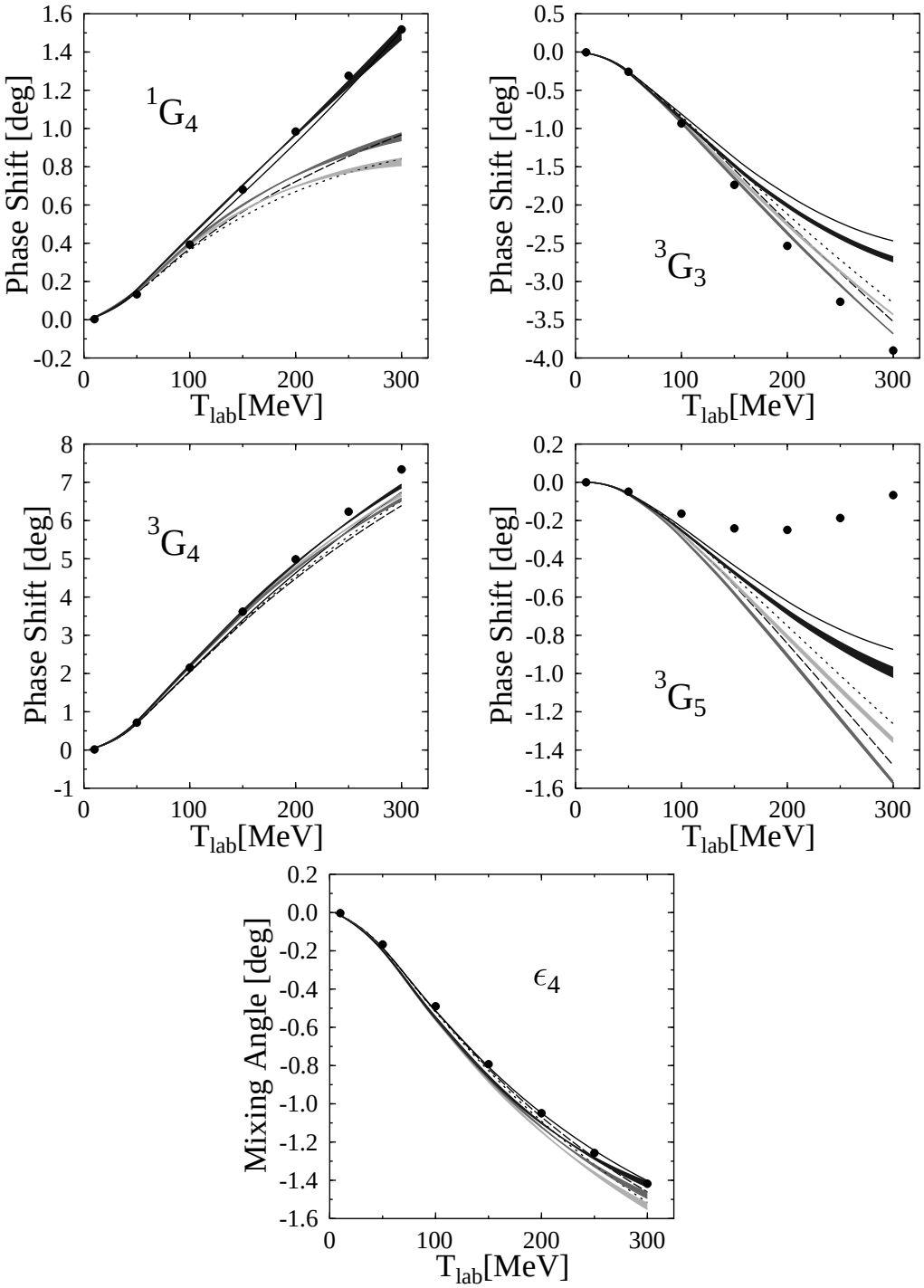

Figure 6.6: The G waves and the ϵ_4 mixing angle. The curves have the same meaning as in Fig. (6.4).

	OPE			NLO			NNLO		
Λ^2(GeV^2)	1.67	1.01	0.62	1.67	1.01	0.62	1.67	1.01	0.62
$^3D_1$	-16.96	-16.67	-16.03	-18.63	-18.24	-17.38	-3.44	-6.43	-8.80
$^1D_2$	1.98	1.77	1.40	3.26	2.96	2.42	10.93	9.63	7.74
$^3D_2$	19.52	19.81	17.53	18.78	18.32	17.34	21.61	20.94	19.56
$^3F_2$	1.91	1.92	1.92	1.67	1.69	1.71	1.92	2.00	2.05
ϵ_2	-4.73	-4.50	-4.06	-4.11	-3.93	-3.56	-3.74	-3.55	-3.17
$^1F_3$	-3.56	-3.53	-3.39	-3.69	-3.66	-3.52	-3.39	-3.35	-3.22
$^3F_3$	-3.26	-3.28	-3.25	-3.18	-3.19	-3.15	-2.27	-2.29	-2.31
$^3D_3$	-4.06	-4.09	-4.10	-6.17	-5.97	-5.65	3.38	1.89	0.29
$^3G_3$	-2.17	-2.20	-2.24	-2.27	-2.31	-2.35	-1.91	-1.94	-1.99
ϵ_3	6.55	6.55	6.44	6.68	6.68	6.56	6.23	6.24	6.16
$^1G_4$	0.69	0.69	0.70	0.74	0.75	0.76	0.95	0.96	0.98
$^3G_4$	4.64	4.70	4.77	4.58	4.64	4.71	4.74	4.80	4.87
$^3F_4$	0.56	0.57	0.58	0.64	0.64	0.65	1.69	1.65	1.56
$^3H_4$	0.31	0.32	0.33	0.30	0.31	0.32	0.33	0.33	0.34
ϵ_4	-1.12	-1.13	-1.14	-1.09	-1.11	-1.12	-1.07	-1.08	-1.10
$^3G_5$	-0.77	-0.78	-0.80	-0.87	-0.88	-0.90	-0.64	-0.65	-0.67

Table 6.3: Cut-off dependence of the peripheral-waves phase-shifts at T_{lab}=200 MeV. Results at the OPE, NLO and NNLO are shown.

originates in the NNLO diagrams. The $\Lambda \to \infty$ and the DR calculations are not identical. As explained in [164] one has

$$\begin{aligned} W_{DR} &= W_{DR}^{(non-pol.)} + W_{DR}^{(pol.)}, \\ W_{CO} &= W_{CO}^{(non-pol.)} + W_{CO}^{(pol.)}, \\ W_{CO}^{(non-pol.)} &\stackrel{\Lambda\to\infty}{\longrightarrow} W_{DR}^{(non-pol.)}. \end{aligned} \tag{6.19}$$

The two polynomial terms have a similar structure, with the cut-off mass Λ and the renormalization scale μ interchanged and different coefficients for the monomials. The difference between the two is given by short range contact potentials. The difference between the Λ^2=1.672 GeV^2 and DR calculations is sizeble for the D waves, which are sensitive to contact potentials with four derivatives or more, amounting up to half of the observed difference between the DR and low-cut-off calculations ($^3D_1$ and $^3D_3$). The situation is totally different for the F waves and higher for which this difference is small (with the exception of the $^3F_2$ wave).

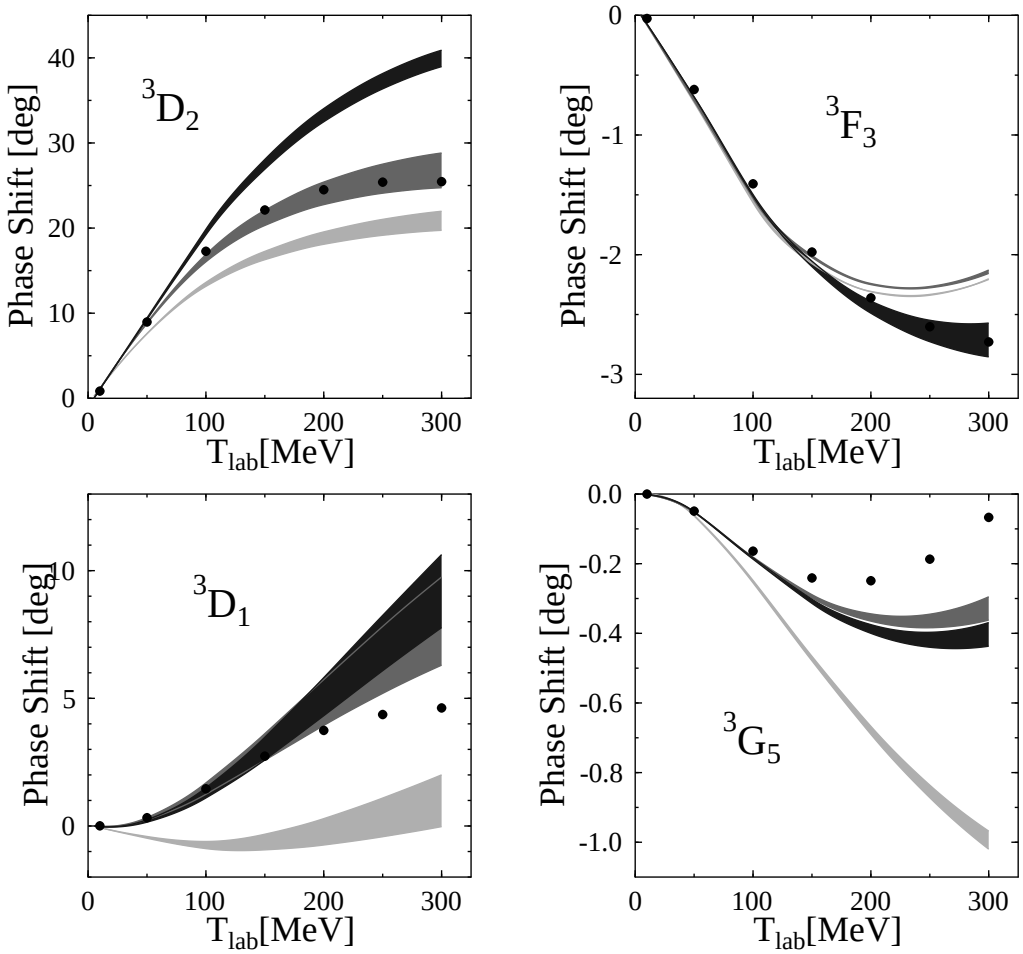

Figure 6.7: Selected waves for which the effect of the iteration of the quasipotential is shown (dark-grey band). The Born term result is represented by the light-grey band. The effect of adding the once iterated one-pion exchange term to W is also shown (grey band).

6.4 Effect of the iteration of the potential on the phase shifts

In the previous section the phase shifts have been computed by approximating the scattering matrix by the Born term. As already mentioned this is expected to be a reasonable approximation when the value of the phase shift is small and for the higher partial waves. Nevertheless, for certain waves ($^3D_2$,$^3D_1$, $^3F_2$ and $^3G_5$) differences with respect to the experimental np phase shifts were observed, some of the phase shifts being numerically

small. In this section we address the question whether this difference can be explained by a nonperturbative character of those channels. We have therefore iterated the BSLT equation and extracted the resulting phase shifts, some of them being plotted in Fig. (6.7).

Besides the effect of iteration, the effect of adding only the once iterated one-pion exchange term to the quasipotential has also been plotted. It can have an important impact on the value of the phase shifts of certain waves, contrary to what is stated elsewhere [164]. Adding it results in a improvement of all phase shifts for which the Born approximation showed a difference when compared with the experimental values. Three such examples are plotted in Fig. (6.7): compare the light-grey and grey bands. Not shown here is the case of the ${}^3D_1$ partial wave for which the inclusion of the iterated one-pion exchange leads to a dramatic change in the value of the phase shift which decreases by 20° at 300 MeV.

Iterating the potential increases somewhat its value to reach the value $\delta_{{}^3D_1}$=-20 ° at 300 MeV, a much better situation than the one presented in Fig. (6.4). Other waves that show a closer resemblance to the experimental data after the quasipotential equation is solved are: ${}^3D_3$,${}^3F_3$,${}^3G_3$ and ${}^3G_5$. For ${}^3F_2$, another problematic partial wave, although the change is in the good direction it is only marginal, while for the ${}^3D_2$ the situation has worsened (see Fig. (6.7)). This is the only partial wave that at this stage still shows a sizable difference with the experimental data.

6.5 Numerical accuracy of the results

In our calculation numerical inaccuracies can originate from two sources: first the finite accuracy to which the scalar loop integrals are computed using the ff libraries and second our method for treating the cut-off integrals. Of course, in the case of DR only the former source appears.

The ff [128] libraries have been developed for the evaluation of scalar loop integrals one encounters in particle-physics calculations. It is based on more refined numerical algorithms than its predecessor $FORMF$ [126] written by M. Veltman to perform the same task. The ff package is delivered with built in error evaluation routines. Unfortunately these routines have proved unreliable in our case and to determine the numerical accuracy we have resorted to an explicit comparison between the outputs of ff and $FORMF$. This has been done for a few relevant kinematical cases characteristic for our particular model. In all cases the outputs of the two programs have been identical up to 8 digits or more.

The second source of inaccuracies has proved to be the most severe one. We remind that in our model each meson propagator is multiplied with a dipole form factor. Since the ff program can only handle four-point functions or lower the following reduction has to be applied to each of the them:

$$\begin{aligned}\frac{1}{k^2-m_\pi^2}\left[\frac{\Lambda^2}{k^2-\Lambda^2}\right]^2 &\approx \frac{1}{k^2-m_\pi^2}\,\frac{\Lambda^2}{k^2-(\Lambda^2-\varepsilon)}\,\frac{\Lambda^2}{k^2-(\Lambda^2+\varepsilon)} \\ &= \frac{\Lambda^4}{\Lambda^2-m_\pi^2}\left[\frac{1}{2\varepsilon}\left(\frac{1}{k^2-(\Lambda^2+\varepsilon)}-\frac{1}{k^2-(\Lambda^2-\varepsilon)}\right)\right.\end{aligned} \tag{6.20}$$

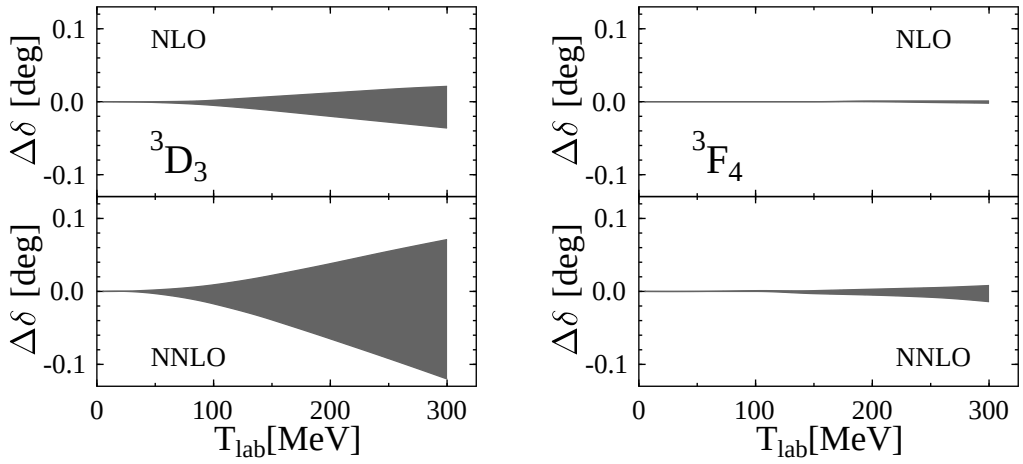

Figure 6.8: The sensitivity of the phase shifts to the variation of the ε parameter. NLO and NNLO results are shown separately.

$$-\frac{1}{\Lambda^2 - m_\pi^2}\left(\frac{1}{k^2-\Lambda^2} - \frac{1}{k^2-m_\pi^2}\right)\Bigg].$$

The approximation in the first line becomes an identity when ε approaches zero. As can easily be seen from the second line this limit leads to strong cancellations which can lead to a severe loss of accuracy. Very small values for ε are thus counterproductive, but so are "large" values since in that case the approximation in the first line becomes poor. Varying ε from very small to "large" for a specific range of values, a plateau can be reached where the accuracy is maximal. In the actual calculations the value ε=0.044 GeV^2 has been used. This value is towards the right edge of the maximum accuracy plateau and has been proved that this can be used with reasonable accuracy for all the cases of interest here. To show the sensitivity of our results with respect to the variation of this parameter we have varied it in the range 0.022...0.066 GeV^2. In Fig. (6.8) the differences between these to extreme cases and the ε=0.044 GeV^2 one has been plotted for two representative phase shifts for the NLO and the full result. The difference grows with energy (similar to the cut-off sensitivity) and is biggest for the the D waves (up to 0.1°). It is much smaller for F waves and for the higher waves is practically zero. Modifying the range of variation for ε to 0.009...0.088 GeV^2 the difference shows an important increase indicating that the maximum accuracy plateau has been left.

6.6 The lower partial waves

For the description of the lower partial waves a proper consideration of the short-range nucleon-nucleon interaction is required. In effective field theories for the NN interaction, like chiral perturbation theory, short range effects are introduced via contact terms. They

Fit	$g_\pi^2/4\pi$	$g_\eta^2/4\pi$	$g_\varepsilon^2/4\pi$	$g_\rho^{V^2}/4\pi$	g_ρ^T/g_ρ^V	$g_\omega^2/4\pi$	$g_\delta^2/4\pi$	Λ_{OPE}^2	Λ_{TPE}^2
OBE	14.20	3.09	7.34	0.43	6.80	11.00	0.33	1.32	–
Fit1	13.60	3.09	1.90	0.43	5.20	9.00	0.33	2.11	0.53
Fit2	13.60	3.09	3.16	0.60	4.57	8.62	0.33	1.67	0.44
Fit3	13.60	3.09	4.40	0.61	4.64	9.16	0.33	1.67	0.35

Table 6.4: Coupling constants of the original one-boson-exchange model of Fleischer and Tjon (OBE) and for the three fits presented in this section. The values of the cut-offs Λ_{OPE}^2 and Λ_{TPE}^2 are given in GeV^2. For the three fits the values of the LECs given in Table (6.1) have been used.

consist of four-fermion interactions with an even number of derivatives acting upon the nucleon fields. Due to power-counting, at each order in the effective field expansion the number and the form of the contact terms is unambiguously determined. There are two such terms at leading order (LO), corresponding to spin singlet and triplet scattering, seven at NLO and 24 at N^{3}LO. Their matrix elements in momentum space are polynomials of degree 0, 2 respectively 4 in the momentum transfer between nucleons. They will therefore only contribute to the lower partial waves (S,P and respectively D) leaving the peripheral waves unaffected. Because of these terms, a good description of the low partial waves of the NN potential in the chiral models for the strong force is possible. Due to their large number, the values of the contact term coupling constants can be determined from a fit of each partial wave separately or from the effective range expansion (for the $^1S_0$ and $^3S_1$ channels) [32]. Using the NNLO TPE derived by Kaiser [33], Entem *et al*. [174, 175] have shown that for a good reproduction of the NN phase shifts below 300 MeV short range contact interactions are required in the D waves. Once the N^{3}LO contact terms were used (which contradicts the philosophy of chiral perturbation theory) a reproduction of all partial waves was possible. Later [38, 39], the consideration of all the N^{3}LO contributions to the potential, derived by Kaiser [34, 35, 36, 37, 176] (which besides one loop TPE contributions also contains two-loops terms), has allowed the construction of a charge-dependent chiral potential of similar quality [39] as the more conventional ones [19]. In [165] Epelbaum has shown that using a sharp cut-off procedure, which removes the unnatural short range part of the chiral NN potential at NLO, a qualitatively good description can be achieved for all the partial waves, provided the values of both the cut-off used to regularize the two-pion exchange loops and the one used to regularize the Lippmann-Schwinger equation are chosen in the 500...800 MeV range. It is stated [165] that partial waves with deficiencies at NNLO are improved if within the same formalism also the N^{3}LO terms of the potential are included. A pioneering work in this direction has been performed by Ordónez and coworkers [30] who have included at NNLO both TPE and Δ isobar contributions and then solved the Schrödinger equation in coordinate space.

A second possibility for representing the short range physics lies in the OBE representation of the nucleon-nucleon potential. The short range repulsion of the nucleon-nucleon is mimicked by the exchange of the ω meson. In Section (6.2) similarities of the TPE po-

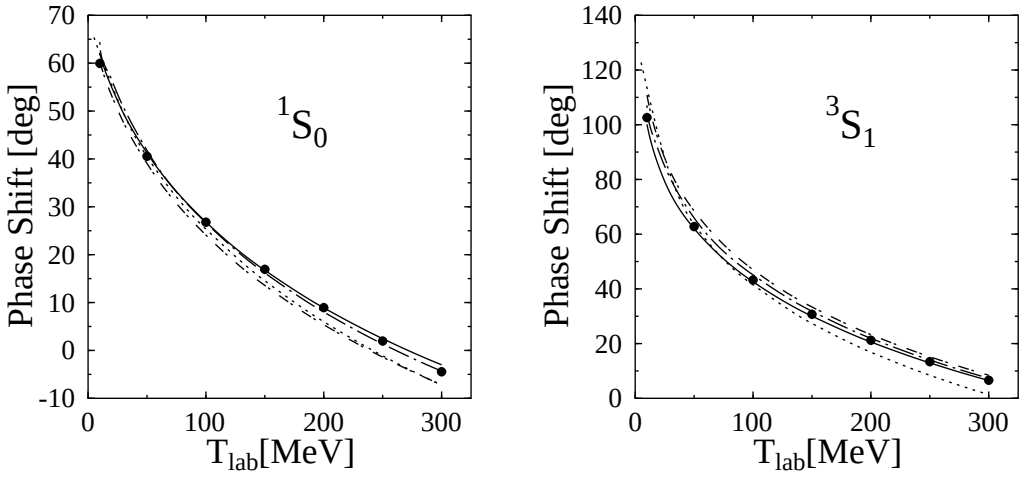

Figure 6.9: The S waves obtained from solving the $BSLT$ equation are plotted for a comparison with the experimental phase shifts of the PWA93 analysis (full circles) and the OBE model of Fleischer and Tjon (dotted line). The three parameter sets presented in Table (6.4) (Fit1,Fit2 and Fit3) give rise to results plotted here by the full, dashed-dotted and short dashed-dotted lines respectively.

---

tential and that of the σ and ω mesons have been presented. It is expected that the TPE potential will be a substitute for the medium range contributions of these two mesons to some extent. In an attempt to describe the low partial waves of NN scattering it is thus natural to consider the nucleon-nucleon potential as the sum of the OBE and TPE terms. In order to achieve agreement with the experimental phase shifts the meson-nucleon coupling constants and cut-off values have been varied, with the expectation that coupling constants like the one of the σ meson will substantially decrease, given the fact that the medium range attraction is now included via TPE terms. Approaches similar to ours have been used before. We have already mentioned the work of Partovi and Lomon [13] who have considered the direct and crossed box contributions to the potential. More recently, Zuilhof [127, 177] has considered besides the two-pion direct and the crossed box the corresponding π-ω boxes. These latter contributions were included in order to weaken the short range effects of the two-pion diagrams. In particular, they play an important role in obtaining the correct S waves splitting. Kaiser *et al.* [178] has added tree-level contributions from the ω, ρ and η mesons along with two-pion exchange loops with intermediate Δ isobar states to the two-pion-exchange diagrams and studied the peripheral waves. Unfortunately a significant improvement of the D waves with respect to [33] has not been achieved.

Returning back to our model, we should first mention that the BSLT equation has been iterated by keeping only the positive intermediate states, *i.e.* the matrix elements of the potential between negative and mixed negative-positive energy states has been set to zero. Nevertheless in evaluating the one-loop terms representing the TPE po-

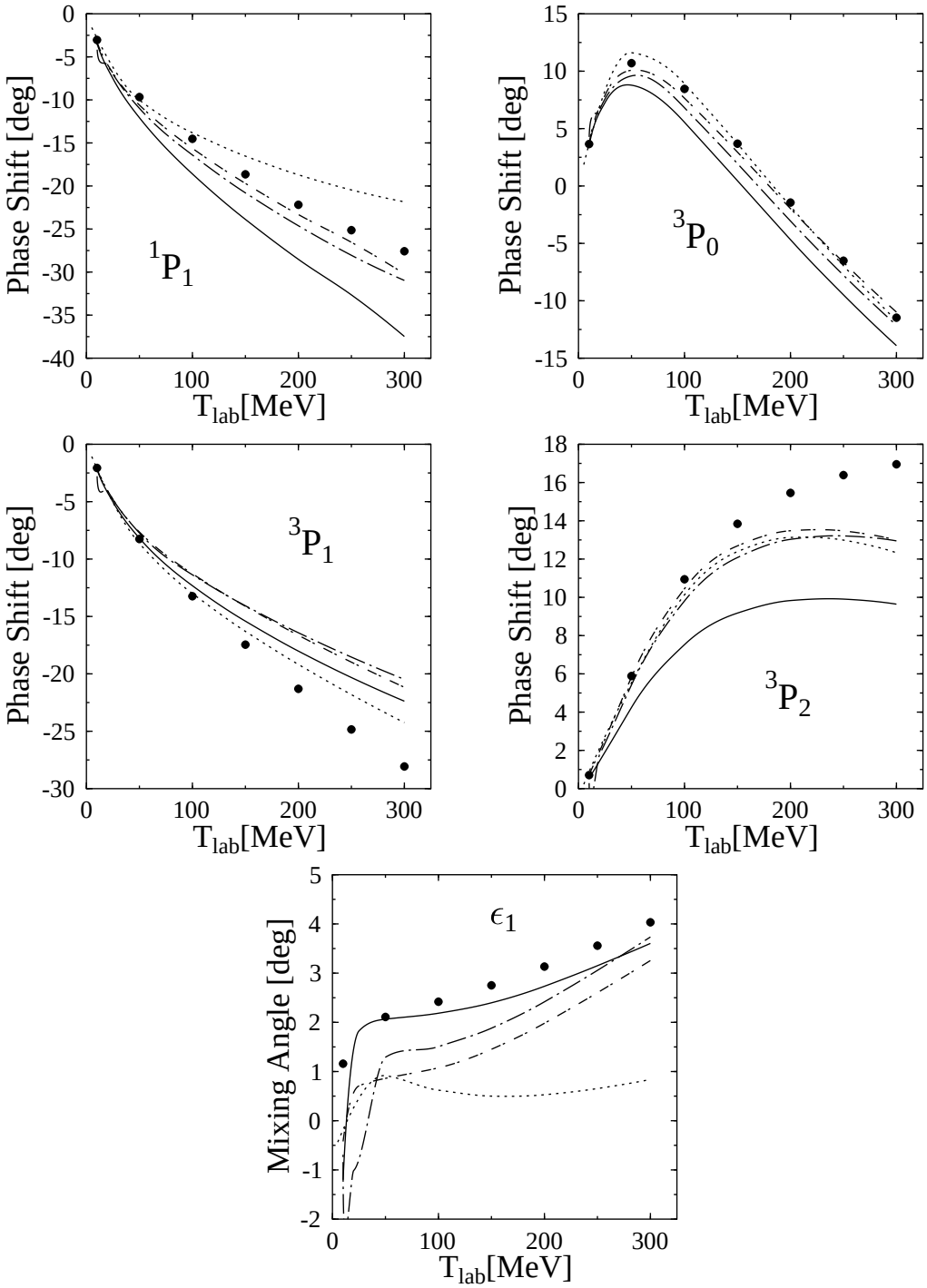

Figure 6.10: The same as in Fig. (6.9) but for the P waves and the mixing-angle ϵ_1.

tential, propagation of the intermediate negative-energy states has been allowed. The corresponding terms are expected to contribute little, due to the pseudovector nature of the pion-nucleon coupling (negative energy states are suppressed at πN vertices). At the level of quasipotential there are now three cut-off parameters: Λ_{OPE} for the OPE potential, Λ_{TPE} used to regularize the TPE one-loop contributions and Λ_H used in the construction of the heavy-meson potential. The last one has been kept fixed, Λ_H^2=1.32 GeV^2, while the other two have been varied (see Table (6.4)). Due to the wrong short-range behavior of the potential the BSLT equation is regularized by a second form-factor, of dipole form, with the value of the cut-off kept fixed at $\tilde{\Lambda}^2$=1.32 GeV^2. In line with the observed sensitivity for the peripheral waves (especially D waves) the value of the cut-off needed to regularize the one-loop contributions has been varied. Varying any of the cut-off parameters necessitates a refit of the whole model, since the values of the low energy NN scattering parameters (scattering lengths and effective ranges) are modified by this operation. We have not varied Λ_{TPE} continuously but rather picked three distinct values Λ^2=0.35, 0.44 and 0.53 GeV^2 for which we show results.

The results we present in this section are preliminary, *i.e.* we have not performed a full scale fit of the model to the experimental data but rather used the following procedure. The value of the S waves phase shifts has been first brought in close agreement with the experiment at an arbitrary chosen lab energy, usually T_{lab}=200 MeV, by varying the g_ε, g_ρ^V and g_ρ^T and if necessary g_ω "by hand". The first three couplings are important for the determination of the overall strength and splitting of the S waves. Then an automatic search, similar to the χ^2 fitting method, for the meson coupling constants was performed. Because of the appreciable CPU time required only the above mentioned couplings have been varied in the process. The remaining (g_π, g_η and g_δ) as well as the LECs have been kept fixed. The values in [127] (fit A) for $g_\eta^2/4\pi$ and $g_\delta^2/4\pi$ have been used while for the pion-nucleon coupling constant the more recent value $g_\pi^2/4\pi$=13.60 has been chosen (see Table (6.4)). Only the S and P waves have been fitted to the corresponding experimental data at three values for T_{lab}: 20, 100 and 200 MeV. The values of the coupling constants for these three fits (labeled Fit1, Fit2 and Fit3) are shown in Table (6.4). Each of these fits corresponds to a different value of the pion-loop cut-off Λ_{TPE}, chosen in line with the observed cut-off dependence of the peripheral waves (especially D waves).

The first thing to remark from Table (6.4) is the considerable decrease of the g_ε coupling constant with respect to the OBE model value, especially for higher values of Λ_{TPE}. When it Λ_{TPE} is decreased too much of the attractive central piece of the TPE potential is cut off leading to the need for an increase of g_ε. The maximum value for the pion-loop cut-off is correlated with the σN coupling constant. Choosing a too high value for the former results in $g_\varepsilon^2/4\pi$=0.0 in the early stages of the fit and in the impossibility of reproducing the experimental values of the phase shifts. Values for Λ_{TPE}^2 starting at 0.7 GeV^2 have been found to be problematic. The changes of the ρ meson coupling constants are not of the same relative magnitude, due to the fact the the isovector tensor and spin-spin potentials produced by the TPE contributions are relatively not as important as the isoscalar central with respect to their OBE counterparts. We also note the reduction of the g_ω coupling constant with 20%.

The resulting phase shifts for the three different fits are shown in Fig. (6.9), Fig. (6.10)

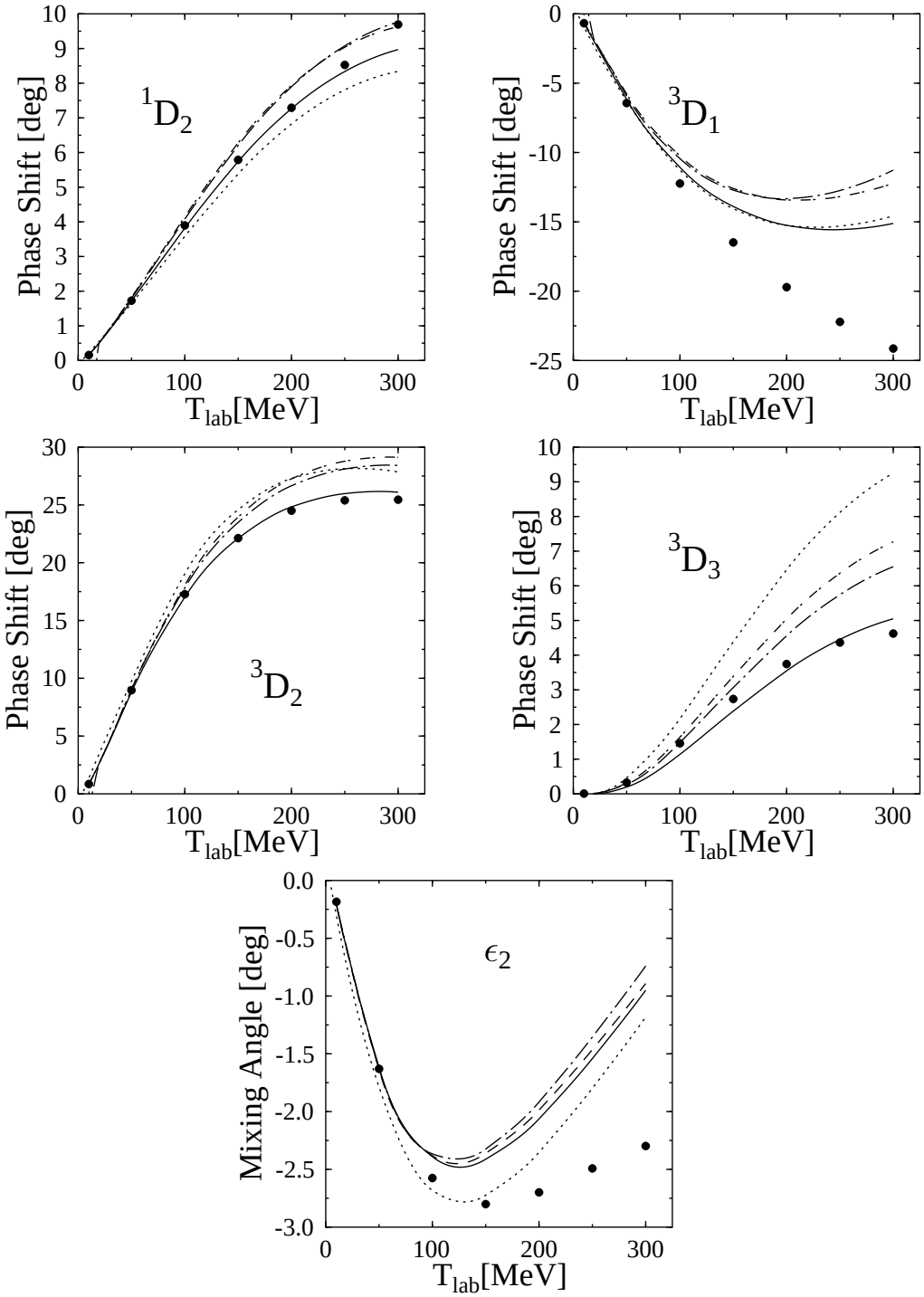

Figure 6.11: D waves and the mixing-angle ϵ_2. The meaning of the curves is the same as in Fig. (6.9).

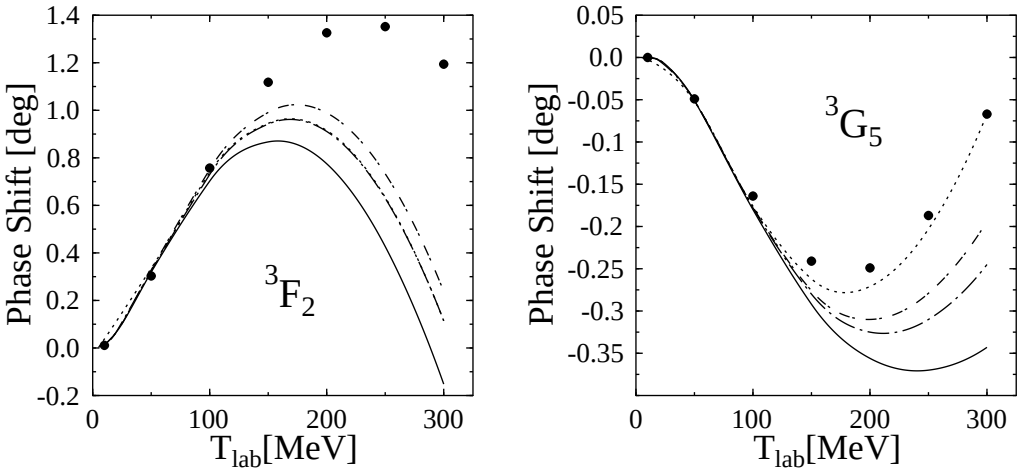

Figure 6.12: Selected higher partial waves.

and Fig. (6.11) for the S, P and D waves respectively. For comparison the OBE phase shifts are also plotted. The S waves are reproduced rather well especially for the Fit1 and Fit2 set of parameters. The Fit3 set shows deviations of the order of 5° for both waves. The deviations of the OBE model from the data is of similar magnitude. We remind that the low energy parameters of the NN force have not been fitted here and deviations even at low energy are normal under these circumstances, given the nonperturbative character of these two channels.

In spite of the fact that the P waves have been among those fitted, their reproduction is only qualitatively. All of them (with the exception of $^3P_0$) deviate with 5-10° at 300 MeV. The quality of the TPE+OBE potential is similar to that of the OBE model. Moreover, the ϵ_1 mixing parameter as described by Fit1 is in remarkable agreement for such a simple fit. Taking any of the set of parameters in Table (6.4) and modifying Λ_{TPE} within the range used for the peripheral waves, while keeping all the other coupling constants fixed, shows a great sensitivity for all P waves with the experimental points within or close proximity of these bands. S waves are extremely sensitive to this procedure too. It suggests that a careful fit might lead to an important improvement of their description. The OBE description of the $^1P_1$, $^3P_2$ and ϵ_1 is equally modest.The NNLO chiral model of Epelbaum *et al.* shows a similar strong cut-off dependence of the P waves, with some of them ($^1P_1$,$^3P_0$ and ϵ_1) reproduced only qualitatively. The N^{3}LO version of the chiral model [38, 39] manages to easily reproduce all these waves accurately partly due to the abundance of contact terms that correct the short range potential and their associated free parameters (LECs) being determined in the process of fitting.

D waves have not been among the fitted ones, since the effects of the heavy mesons is supposed to be less important. This is not completely true since by looking at the curves produced by Fit1 and important improvement of 15° is noted for the $^3D_2$ partial wave as compared with the pure TPE results. For this particular fit also $^3D_3$ is in excellent agreement with the experimental values. Out of the D waves $^3D_1$ shows the

	Fit1		Fit2		Fit3	
	OPE+TPE	FULL	OPE+TPE	FULL	OPE+TPE	FULL
$^3D_1$	−17.79	-15.25	−16.58	-13.33	−17.25	-13.42
$^1D_2$	8.20	7.27	7.10	7.90	5.94	7.93
$^3D_2$	34.25	24.83	32.49	26.67	31.70	27.26
$^3F_2$	1.70	0.78	1.66	0.91	1.64	1.00
ϵ_2	-1.58	-2.06	-2.61	-1.92	-3.38	-1.99
$^1F_3$	-3.38	-3.92	-3.39	-3.77	-3.41	-3.67
$^3F_3$	-2.43	-2.77	-2.50	-2.65	-2.57	2.60
$^3D_3$	5.23	3.55	4.32	4.56	3.52	5.05
$^3G_3$	-2.61	-2.47	-2.62	-2.44	-2.60	-2.40
ϵ_3	5.97	5.69	6.00	5.60	6.04	5.71
$^1G_4$	0.94	0.97	0.93	1.00	0.92	1.02
$^3G_4$	4.95	4.90	4.97	4.97	4.95	4.99
$^3F_4$	1.56	1.38	1.49	1.55	1.37	1.64
$^3H_4$	0.31	0.30	0.31	0.30	0.31	0.35
ϵ_4	-1.08	-1.06	-1.09	-1.07	-1.09	-1.07
$^3G_5$	-0.39	-0.36	-0.40	-0.33	-0.42	-0.31

Table 6.5: The importance of the heavy-meson-exchange contributions to the peripheral waves can be determined from a comparison between the full model (OPE+TPE+OBE) and the model restricted pions exchanges only (OPE+TPE). Phase shifts for each of the three new parameter sets in Table (6.4) at T_{lab}=200 MeV are shown.

poorest description. It has been possible to bring it close to the experimental value at the expense of worsening the description of the $^1P_1$ (which is already poorly described) and of the ϵ_1 parameter. In the case of Ref. [165] all the D waves with the exception of $^3D_3$ are reasonably described. Out of the higher partial waves we have selected only two of them, presented in Fig. (6.12). $^3F_2$ was one of the partial waves that has not been properly described by the pure TPE potential Fig. (6.5), the experimental value being overshot by theory. Including the OBE provides too much attraction in this channel, the experiment being now underestimated by a similar amount. The new theoretical values resemble the old OBE model, meaning that the TPE potential is canceled by the change in the OBE model (mainly σ attraction reduction). The other high partial waves shown here, $^3G_5$, differs very little from the TPE result of the previous section. Similar conclusions hold for the other high partial waves as can be seen from Table (6.5) in which the importance of the heavy-meason exchanges at T_{lab}=200 MeV is shown. We present phase shifts extracted from the full model (for each of the three fits) and the model with contributions only from the pion (OPE and TPE). Heavy-meson contributions are still sizeble for the D waves and for the $^3F_2$ partial wave. The behavior of the latter can be understood from the fact that it belongs to a coupled channel, together with $^3P_2$.

6.7 Summary

Results for the elastic NN scattering phase shifts below 300 MeV have been presented in this chapter. The peripheral waves (D and higher) are described reasonably well by the chiral symmetry constrained TPE interaction as soon as a low value for the one-loop cut-off is adopted. This is necessary in order to reduce to appreciable isoscalar central attraction generated by the irreducible two-pion exchange graphs. A few of the peripheral waves show a nonperturbative character, contrary to common belief, and all of them, with the exception of $^3D_3$, are being improved upon the iteration of the potential. The TPE potential mimics the isoscalar central potential generated by the fictitious σ meson and to a lesser extent the isovector tensor and spin-spin potential. This is supported by the conclusion resulting from a resonance saturation model that the values of the low energy parameters c_1, c_3 and c_4 are determined by mesons (σ and ρ) and baryons (Δ), degrees of freedom which are integrated out. In support of that the OBE potential is added to the TPE one and the resulted model is "fitted" using a simple parameter search procedure to the experimental low partial waves (S and P). This proves difficult and while the S waves are reproduced with reasonable accuracy, most of the P waves are reproduced only qualitatively (difference of up to 10° at 300 MeV). An important decrease of the g_ε coupling constant is observed, in support of the conclusion that the medium range attraction is properly generated by the chiral two-pion exchange loops with a low cut-off. Similarly the TPE graphs give about half of the needed medium range isovector tensor and spin-spin potential judging from the change in the ρ meson coupling constants during the process of fitting. The resulting model is of similar quality as the OBE model of Fleischer and Tjon. For an accurate description important improvements are required, unlikely to come just from an improvement of the preliminary fit presented here.